IOSR Journal of Biotechnology and Biochemistry (IOSR-JBB)
ISSN: 2455-264X, Volume 10, Issue 6 Series 1 (Nov. – Dec. 2024), PP 01-07
www.iosrjournals.org

Prediction Of Wheat Flour Gelatinization Characteristics Using Hyperspectral Imaging Technology

Denglin Qiu, Fei Hao, Tao Liu, Zhuoyuan Zhang
Shandong Seed Industry Group Co., LTD, Yinfeng Fortune Plaza, Jinan City, Shandong Province

Abstract
Wheat was one of the most widely cultivated and economically significant staple crops globally. Wheat flour was a primary ingredient in various foods, with its quality commonly described by parameters such as moisture, protein, starch, ash, gluten content, and gelatinization characteristics. Understanding these parameters was essential for assessing wheat flour's processing suitability and selecting the appropriate wheat flour type for specific food formulations. This study leverages hyperspectral imaging (HSI) technology to predict the gelatinization characteristics of wheat flour, using peak viscosity as a key indicator. Partial Least Squares Regression (PLSR), Principal Component Regression (PCR), and Support Vector Machine Regression (SVMR) models were established based on raw spectral data and nine different preprocessing methods. Among these, the Standard Normal Variate (SNV) preprocessing method yielded the best prediction results. Considering model speed, robustness, and stability, the optimal model for predicting wheat flour peak viscosity was the SNV-IVISSA-IRIV-SVMR, achieving $R^2 = 0.8955$ and RMSEP = 115.4859 cP. This approach enables accurate prediction of wheat flour gelatinization characteristics, offering valuable theoretical support for wheat flour processing and manufacturing.

Keywords: *Hyperspectral imaging; Wheat flour; Near-infrared; Gelatinization characteristics*

Date of Submission: 09-11-2024 Date of Acceptance: 19-11-2024

I. Introduction

Wheat is an economically important crop for both human consumption and animal feed [1]. Wheat flour is a key ingredient in various food products, with quality parameters such as protein, starch, moisture, gluten, ash, fat content, and gelatinization characteristics being critical indicators of its quality [2,3]. Understanding these parameters is essential for evaluating the processing characteristics of wheat flour and selecting the appropriate type for different food formulations. These parameters are closely linked to the processing properties and nutritional quality of wheat flour. As noted, protein, starch, moisture content, gelatinization characteristics, and deoxynivalenol levels significantly impact the final cost, processing suitability, and storage stability of wheat flour [4]. Traditional chemical testing methods, while accurate and reliable, are destructive and resource-intensive, particularly when analyzing large sample volumes, requiring substantial time, labor, and chemical usage. Therefore, there is a need to develop an efficient, cost-effective, non-destructive, and accurate quality evaluation system for the food industry.

In recent years, spectroscopic analysis techniques have been widely employed for quality assessment of agricultural products. Wang et al. [5] utilized hyperspectral imaging (HSI) to extract average spectral data from millet flour, employing the Sparrow Search Algorithm (SSA) to optimize the Backpropagation (BP) algorithm for predicting gelatinization characteristics, taking peak viscosity as an example. Results demonstrated that the SSA-optimized BP algorithm enhanced prediction accuracy for millet flour gelatinization properties, reducing the mean square error (MSE) from 0.0266 to 0.0175 compared to the BP algorithm alone. This study provides theoretical support for the use of HSI combined with deep learning to predict gelatinization characteristics in millet flour. Wu et al. [6] acquired diffuse reflectance spectra of millet in the 370-1020 nm range and used a Rapid Visco Analyzer (RVA) to measure seven gelatinization indices. Following spectral preprocessing with Savitzky-Golay (SG) smoothing, Multiplicative Scatter Correction (MSC), and first derivative transformation, the authors employed the Successive Projections Algorithm (SPA) to select feature wavelengths and establish a Multiple Linear Regression (MLR) model.

For peak viscosity, minimum viscosity, and setback values, 9, 17, and 18 feature wavelengths were extracted, yielding predictive correlation coefficients (RP) of 0.9347, 0.8255, and 0.8746, respectively. This study demonstrated that visible-near infrared (VIS-NIR) spectroscopy can effectively assess millet gelatinization characteristics in a non-destructive manner, indicating potential for practical applications. Spectroscopic

analysis offers advantages of speed and non-destructiveness, overcoming the limitations of traditional destructive testing methods. In recent years, hyperspectral imaging (HSI) has emerged as a highly promising technology for non-invasive, contamination-free quality evaluation of food products [7-9]. Combining the benefits of spectroscopy and imaging, HSI can simultaneously capture the physical and chemical information of wheat flour.

HSI technology operates across a wide spectral range (780-2500 nm), with the specific range of 900-2300 nm known as near-infrared hyperspectral imaging (NIR-HSI). Near-infrared spectroscopy establishes the relationship between spectral data and detection indices based on the interaction of light radiation with a sample, particularly through the absorption of molecular overtone and combination vibrations [10-11]. NIR-HSI extracts spatial and spectral information from captured images, providing a characteristic chemical map for each pixel associated with this information. By acquiring a three-dimensional data matrix containing thousands of consecutive images, narrowband spectra, and two-dimensional spectral information, NIR-HSI overcomes the limitations of traditional spectroscopy [12-13].

This study focuses on various wheat flour types, aiming to develop a non-destructive method for detecting wheat flour gelatinization characteristics using HSI technology. Gelatinization characteristics of different wheat flour varieties were measured with a Rapid Visco Analyzer (RVA), using peak viscosity as a key indicator for prediction. Prediction models were established by integrating spectral data, including models based on raw spectral data as well as models using preprocessed data. Feature wavelength extraction algorithms—such as the Successive Projections Algorithm (SPA), Competitive Adaptive Reweighted Sampling (CARS), Uninformative Variable Elimination (UVE), Interval Variable Iterative Space Shrinking Analysis (IVISSA), and Iterative Retain Information Variable (IRIV)—were applied to develop the optimal prediction model. This approach effectively predicts peak viscosity and enables accurate detection of gelatinization characteristics in wheat flour.

II. Materials And Methods

Sample preparation

In this experiment, a total of 77 wheat flour varieties were collected, of which 65 were cultivated by Shandong Seed Industry Group Co., Ltd., and 12 were purchased from major supermarkets in Zibo. Each wheat flour type was divided into six parallel samples. Six 300-gram samples were taken from each variety and placed in six clean petri dishes. After capturing hyperspectral images, each parallel sample was divided into three equal parts by weight. Gelatinization characteristics were measured using a Rapid Visco Analyzer (RVA), with each parameter measured three times to calculate an average value. Consequently, 462 wheat flour samples were analyzed, and a library of 462 hyperspectral wheat flour images was constructed.

Hyperspectral image acquisition

Hyperspectral images of the samples were acquired in reflection mode using a laboratory line-scan NIR-HSI system (spectral range: 900-2500 nm) [14]. A charge-coupled device (CCD) camera was used to capture two-dimensional images of the samples by translating the sample across the objective stage. This setup enabled the collection of spatial and spectral information along the spatial-spectral axis based on the reflected light from the samples. The HSI system included a dark chamber, motorized translation stage, near-infrared spectrometer, CCD camera, halogen lamps, and a computer.

Black and white calibration

To remove irrelevant interference and stabilize the acquired spectral data, black and white calibration was performed. The spectral information of a white reference panel with 0.99 reflectance (Specim, Finland) was recorded as I_{white}. Additionally, spectral data were collected with the CCD camera lens covered to obtain I_{dark} [15]. The calibration was calculated using the following formula:

$$R_T = \frac{I_{\text{raw}} - I_{\text{dark}}}{I_{\text{white}} - I_{\text{dark}}} \qquad (1)$$

where R_T represents the calibrated image, I_{raw} is the original sample image, and I_{white} and I_{dark} are the images after white and dark calibration, respectively.

Spectral information acquisition and region of interest (ROI) extraction

During sample scanning, equipment adjustments began once the machine temperature reached -60, setting the exposure time to 2.6 ms, the translation stage speed to 13.50 mm/s, and the CCD camera resolution to 384 × 288. For spectral information extraction from wheat flour samples, a masking method was employed to separate wheat flour from the image background. Given the clear spectral contrast between wheat flour and the background, a single-band grayscale image at 1340 nm was used to establish a mask template for the near-infrared hyperspectral image. The OTSU method was applied for threshold segmentation of the captured images [16]. A binary mask was then created for each sample, assigning pixel values of 0 and 1 to represent

background and wheat flour, respectively. The mean spectral value was calculated for each wheat flour pixel, yielding an average spectrum per image, resulting in a total of 462 samples. The spectral information from the wheat flour samples was then concatenated to form the final spectral matrix for model development, with rows and columns representing the number of wheat flour images and wavelengths, respectively.

Sample set division

The wheat flour samples were divided into calibration and prediction sets for multivariate data analysis. The calibration set was used to optimize and build the quantitative model, while the prediction set was used to validate the reproducibility of the optimized results and the developed quantitative model [17]. The Kennard-Stone (KS) algorithm was applied to split the sample set at a 3:1 ratio, maximizing the euclidean distance between system responses for even coverage across multidimensional space. Consequently, 347 samples were selected as the calibration set, and the remaining 115 samples were used as the prediction set. The peak viscosity distribution of gelatinization characteristics in the calibration and prediction sets is shown in Table 1. The calibration set encompassed the variation range of the prediction set samples. These results indicate that the sample set division method was reasonable, providing a representative sample selection for model construction.

Table 1 Statistics reference measurement results of gelatinization properties in wheat flour of the calibration and prediction sets

Subsets	No. of samples	Min	Max	Mean	SD	SEM	CV
Total	462	1681	2956	2583	321.4353	7.8195	0.1244
Calibration set	347	1681	2956	2607	304.5186	5.9117	0.1168
Prediction set	115	1713	2880	2510	364.0376	8.7956	0.145

III. Results And Discussions

Modeling analysis based on full wavelengths and data preprocessing

PLSR, PCR, and SVMR models were developed based on the full-spectrum data of wheat flour and its preprocessed spectral data. The parameters of each model are presented in Table 2. Results indicate that the SVMR model based on full-wavelength data demonstrated superior predictive performance, with R^2_C, R^2_{CV} and R^2_P values of 0.9782, 0.8706, and 0.8058, respectively, and corresponding RMSEC, RMSECV, and RMSEP values of 52.1031 cP, 111.0163 cP, and 157.4127 cP. After SNV preprocessing, the predictive performance of the SVMR model was significantly enhanced, yielding R^2_C, RMSEC, R^2_{CV}, RMSECV, R^2_P, and RMSEP values of 0.9570, 65.6612 cP, 0.7432, 153.6963 cP, 0.8920, and 117.3760 cP, respectively. Compared to the model based on raw spectral data, the prediction set R^2_P improved by 0.0844, effectively increasing the model's accuracy. Therefore, SNV preprocessing was used for subsequent experiments.

Table 2 The result of PLSR、PCR and SVMR based on different pre-processing methods in predicting peak viscosity

Model	pre-processing methods	R^2_C	RMSEC /cP	R^2_{CV}	RMSECV /cP	R^2_P	RMSEP /cP
PLSR	None	0.9313	79.3304	0.7627	149.8175	0.7289	185.9738
	Detrending	0.9077	91.9246	0.7044	165.5892	0.7728	170.2571
	FD	0.6495	179.1629	0.5642	204.5978	0.6267	218.2522
	SD	0.6774	171.8794	0.4984	217.6691	0.5667	235.1208
	SNV	0.9279	81.2756	0.7751	145.0637	0.7719	170.6017
	MSC	0.9268	81.9037	0.7808	144.8999	0.7621	174.2328
	FD-SNV	0.9299	80.1498	0.6239	189.5893	0.6468	212.2748
	SNV-FD	0.9296	80.2648	0.6433	183.4284	0.6094	223.2480
	SNV-Detrending	0.9054	93.0671	0.7302	158.0111	0.7878	164.5480
	SD-SNV	0.8609	112.8775	0.5519	204.3773	0.6842	200.7402
PCR	None	0.6280	184.5900	0.5488	203.8849	0.6223	219.5201
	Detrending	0.6335	183.2011	0.5707	202.4706	0.6069	223.9489
	FD	0.6510	178.7808	0.5510	204.5078	0.6249	218.7734
	SD	0.6291	184.3158	0.4762	222.9345	0.5341	243.8028
	SNV	0.6678	174.4241	0.5783	197.6978	0.6495	211.4684
	MSC	0.7422	153.6535	0.5999	193.2639	0.6761	203.2364
	FD-SNV	0.6372	182.2726	0.4723	223.6384	0.5357	260.5196
	SNV-FD	0.6963	166.7817	0.4875	218.3449	0.4843	256.5152
	SNV-Detrending	0.7299	157.2847	0.6010	196.3128	0.6432	213.362
	SD-SNV	0.7181	160.6826	0.4956	217.5309	0.4776	258.1803
SVMR	None	**0.9782**	**52.1031**	**0.8760**	**111.0163**	**0.8058**	**157.4127**

	Detrending	0.9288	84.1537	0.7796	143.1009	0.8306	147.0324
	FD	0.9738	52.8195	0.7355	155.7700	0.8837	121.7984
	SD	0.9700	58.8465	0.5574	201.5496	0.6654	206.6321
	SNV	**0.9570**	**65.6612**	**0.7432**	**153.6963**	**0.8920**	**117.3760**
	MSC	0.9546	67.8642	0.7501	151.4112	0.8890	119.02178
	FD-SNV	0.9745	55.3020	0.6975	166.7762	0.6462	212.4691
	SNV-FD	0.9749	55.1437	0.7139	162.2037	0.8572	134.9733
	SNV-Detrending	0.9694	54.9476	0.7705	145.5996	0.8847	121.2632
	SD-SNV	0.9720	57.5889	0.5501	203.4631	0.6934	197.7798

Feature wavelength extraction

Hyperspectral image data were characterized by high dimensionality and multicollinearity among bands, containing substantial noise and redundant information. This volume of data requires complex computations, adding strain to the model used for analysis. To improve computational speed, enhance predictive accuracy, and reduce processing time, dimensionality reduction was commonly applied, where specific sensitive or feature wavelengths were selected from the entire spectral matrix to compress the hyperspectral information [18,19]. Feature wavelengths were extracted using SPA, CARS, UVE, IVISSA, and IRIV methods.

Extraction of feature wavelengths based on the SPA algorithm

The SPA was widely applied for selecting feature wavelengths in hyperspectral data [20]. SPA minimizes multicollinearity in the vector space and eliminates redundant information from the spectral matrix. The optimal wavelengths were determined by the subset with the minimum RMSE when calculating the model's RMSE using the SPA algorithm [21]. As shown in Fig. 1(a), the RMSE curve initially drops sharply as the number of selected feature wavelengths increases from 1 to 21. The optimal wavelength position (highlighted in a red box) was reached at 21 wavelengths, corresponding to a minimum RMSE of 116.4289 cP. Fig. 1(b) illustrates the distribution of these 21 selected feature wavelengths, with the x-axis representing the wavelength indices and the y-axis showing reflectance. The selected feature wavelengths were 969, 976, 994, 1032, 1101, 1133, 1258, 1333, 1352, 1383, 1421, 1464, 1599, 1690, 1791, 1867, 1924, 2052, 2090, 2122, and 2164 nm, comprising 10.34% of all bands.

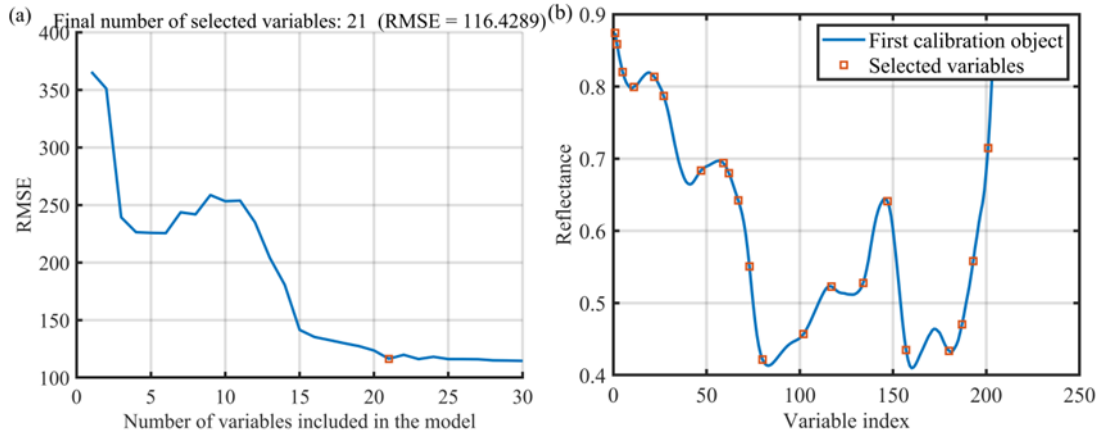

Fig. 1 Selected feature wavelengths by SPA of peak viscosity in wheat flour
(a: RMSE growth pattern of variable, b: sequence number of selected feature wavelengths)

Extraction of feature wavelengths based on the CARS algorithm

To reduce irrelevant spectral information, the CARS algorithm was used to extract feature wavelengths for wheat flour peak viscosity. Spectral data from samples in the calibration set with high peak viscosity were treated as input values. Monte Carlo sampling was performed 250 times, with the number of selected wavelengths determined by RMSECV. Fig. 2 shows the variation trends of the number of wavelengths, RMSECV, and regression coefficient paths as Monte Carlo sampling iterations increase. The feature wavelength extraction process via CARS can be divided into two steps: coarse selection and fine selection (Fig. 2(a)). When the number of iterations was below 80, the number of variables decreases sharply; beyond 80, it stabilizes [22]. The RMSECV decreases as irrelevant wavelengths were removed over iterations 1–80 (Fig. 2(b)), then shows slight variation between iterations 80–91. At 91 iterations, RMSECV reaches its lowest value of 166.9 cP. Beyond 91 iterations, RMSECV increases rapidly due to the removal of wavelengths relevant to peak viscosity, thus stopping the process at this point. In Fig. 2(c), each line represents the regression coefficient path of each variable across sampling iterations. Initially, all regression coefficients were near zero; sampling stops at

iteration 91, where RMSECV was minimized at the * position, as continuing further would remove useful variables. Consequently, 38 feature wavelengths were selected at 91 iterations (969, 976, 982, 988, 1070, 1076, 1082, 1164, 1170, 1177, 1183, 1189, 1346, 1352, 1371, 1377, 1383, 1396, 1402, 1408, 1415, 1421, 1427, 1483, 1489, 1495, 1501, 1726, 1809, 1815, 1826, 1941, 2079, 2090, 2101, 2133, 2143, and 2169 nm), representing 18.72% of the total bands.

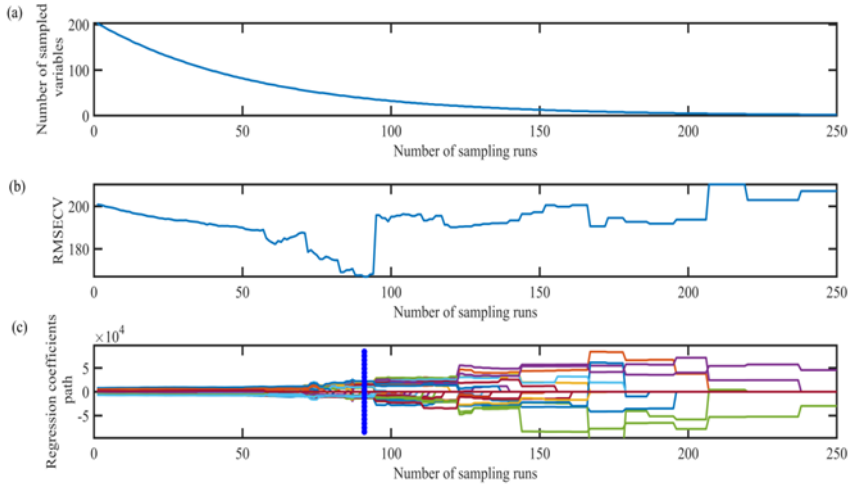

Fig. 2 The process of screening feature wavelengths by CARS of peak viscosity in wheat flour
(a: the number of selected wavelengths in the change process diagram of CARS algorithm, b: RMSECV value changes with the sampling runs, c: the change process of regression coefficient of each variable with sampling times)

Extraction of feature wavelengths based on the UVE algorithm

The UVE algorithm was a variable selection method based on the stability analysis of PLS regression coefficients. It evaluates the stability of each wavelength by analyzing the corresponding regression coefficients in the PLS model, then removes wavelength variables with low absolute correlation coefficients [23]. Fig. 3 demonstrates the stability values of the extracted variables for peak viscosity in wheat flour, with the two horizontal dashed lines indicating the cutoff thresholds. Wavelengths with stability values within these thresholds were excluded as independent variables. The remaining variables, considered relevant, were retained as inputs for the regression model. In this study, UVE selected 47 feature variables from the original 203 wavelengths, representing 23.15% of the total spectral bands.

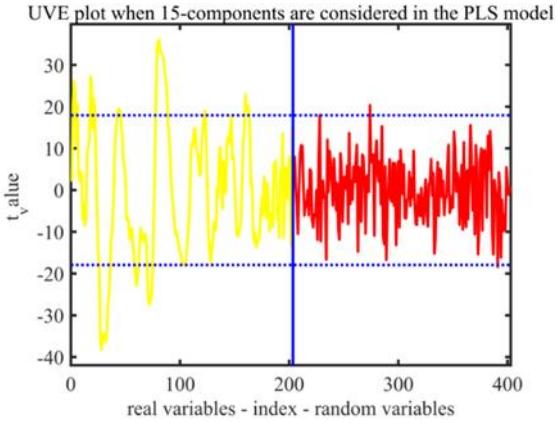

Fig. 3 The process of screening feature wavelengths by UVE of peak viscosity in wheat flour

Extraction of feature wavelengths based on the IVISSA-IRIV algorithm

Relevant wavelengths for peak viscosity in wheat flour were extracted using the IVISSA algorithm, with the process illustrated in Fig. 4. Fig. 4(a) shows the trend of RMSECV over the iterative process, where, after 29 iterations, the RMSECV value decreased to 106.7749 cP, retaining 88 feature wavelengths. The relatively large number of selected wavelengths slowed the model's computational efficiency, making it less conducive to simplification. Therefore, the IRIV algorithm, which performs well in refinement, was applied in combination to further optimize wavelength selection. This combined IVISSA-IRIV algorithm was employed to extract key

wavelengths associated with wheat flour's peak viscosity. Fig. 4(b) presents the optimal set of 20 feature wavelengths, specifically 982, 1076, 1082, 1383, 1390, 1396, 1402, 1408, 1415, 1720, 1844, 1849, 1855, 1861, 1867, 2079, 2101, 2143, and 2164 nm, which account for 9.85% of the total spectral bands.

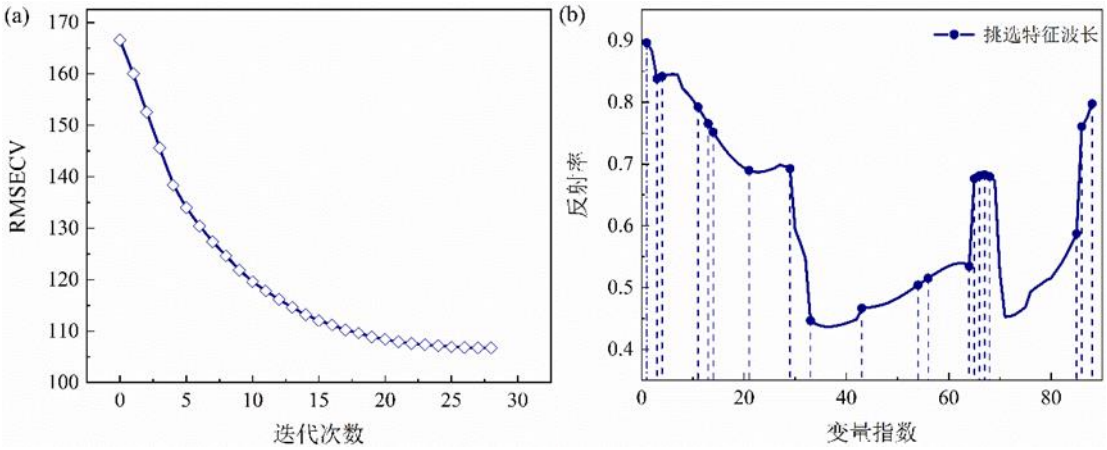

Fig. 4 IVISSA and IVISSA-IRIV algorithms to select feature wavelengths of peak viscosity in wheat flour
(a: variation trend of RMSECV during iterations; b: sequence number of selected feature wavelengths)

Comparison of Optimal Modeling Performance

PLSR, PCR, and SVMR models were constructed using full-spectrum data and spectra with different preprocessing methods. Model performance comparisons showed that SNV preprocessing significantly improved model accuracy. Following feature wavelength extraction with five algorithms—SPA, CARS, UVE, IVISSA, and IVISSA-IRIV—the performance of each model was assessed (Table 3). The SVMR model based on SNV preprocessing and UVE extraction of 47 feature wavelengths demonstrated the best predictive performance, achieving R^2_P = 0.9174 and RMSEP = 102.6580 cP. Comparison with the SNV-IVISSA-IRIV-SVMR model indicated that the IVISSA-IRIV algorithm, selecting 20 relevant wavelengths for peak viscosity, achieved R^2_P = 0.8955 and RMSEP = 115.4859 cP. This approach substantially reduced the number of feature wavelengths while maintaining robust model accuracy. Considering model processing speed and simplification, the SNV-IVISSA-IRIV-SVMR model was identified as the optimal model for characterizing wheat flour pasting properties.

Table 3 the result of PLSR, PCR and SVMR based on different feature wavelengths selection methods in predicting peak viscosity

feature wavelengths selection methods	Model	No.. of wavele-ngths	R^2_C	RMSEC /cP	R^2_{CV}	RMSECV /cP	R^2_P	RMSEP /cP
SPA	PCR	21	0.8583	113.9354	0.7232	161.5495	0.7339	184.2757
	PLSR	21	0.9040	93.7579	0.7905	139.5414	0.8404	142.7217
	SVMR	21	0.9811	49.2858	0.8441	122.4416	0.8080	156.4784
CARS	PCR	38	0.7745	143.6971	0.7129	164.0867	0.6400	214.3074
	PLSR	38	0.8428	120.0017	0.6926	167.6181	0.6371	215.1660
	SVMR	38	0.9794	54.8542	0.8010	137.5365	0.7938	162.2178
UVE	PCR	47	0.4875	216.6452	0.4581	226.9932	0.4812	257.2741
	PLSR	47	0.7327	156.4678	0.5717	202.7371	0.7003	188.9232
	SVMR	47	**0.9654**	**56.5213**	**0.8304**	**127.7976**	**0.9174**	**102.6580**
IVISSA	PCR	88	0.9009	95.2924	0.8257	127.9596	0.6641	207.0222
	PLSR	88	0.9129	89.3135	0.8230	128.2065	0.7009	195.3605
	SVMR	88	0.9694	53.0883	0.8595	114.4387	0.8530	136.9466
IVISSA-IRIV	PCR	20	0.7047	164.4472	0.6673	174.4451	0.6612	207.9132
	PLSR	20	0.7080	163.5217	0.6526	180.4952	0.6608	208.0456
	SVMR	20	**0.9298**	**85.0579**	**0.8185**	**132.3895**	**0.8955**	**115.4859**

IV. Conclusions

In this study, peak viscosity was used as the characteristic index for wheat flour pasting properties. The original spectral data were preprocessed using nine different methods, with SNV preprocessing found to be the

most effective. To simplify model processing, five feature wavelength extraction methods—SPA, CARS, UVE, IVISSA, and IVISSA-IRIV—were applied, extracting 21, 38, 47, 88, and 20 feature wavelengths relevant to peak viscosity, respectively. A comprehensive comparison of model performance in terms of computation speed and stability led to the selection of the SNV-IVISSA-IRIV-SVMR model as the optimal model for wheat flour pasting properties, achieving $R^2_P = 0.8955$ and RMSEP = 115.4859 cP. Using hyperspectral imaging technology to predict wheat flour pasting characteristics, with peak viscosity as a key index, holds significant potential for optimizing wheat flour processing properties, classification performance, and the selection of suitable wheat flour for specific products. Near-infrared hyperspectral imaging offers advantages of being non-destructive, fast, accurate, and stable, and it shows great promise for applications in non-destructive testing of agricultural products.

Acknowledgements

This research was financially supported by the Key Research and Development Program of Shandong Province (Major Scientific and Technological Innovation Project, No. 2020CXGC0108053).

References

[1] Li S, Luo J, Zhou X, Et Al. Identification Of Characteristic Proteins Of Wheat Varieties Used To Commercially Produce Dried Noodles By Electrophoresis And Proteomics Analysis[J]. Journal Of Food Composition And Analysis, 2021, 96: 103685.
[2] Mæhre H, Dalheim L, Edvinsen G, Et Al. Protein Determination—Method Matters[J]. Foods, 2018, 7(1): 5.
[3] Tian W, Chen G, Zhang G, Et Al. Rapid Determination Of Total Phenolic Content Of Whole Wheat Flour Using Near-Infrared Spectroscopy And Chemometrics[J]. Food Chemistry, 2021, 344: 128633.
[4] Caporaso N, Whitworth M B, Fisk I D. Protein Content Prediction In Single Wheat Kernels Using Hyperspectral Imaging[J]. Food Chemistry, 2018, 240: 32–42.
[5] Wang G, Wang W, Cheng K,Et Al. Hyperspectral Imaging Combined With Back Propagation Neural Network Optimized By Sparrow Search Algorithm For Predicting Gelatinization Properties Of Millet Flour[J]. Food Science, 2022, 43(19):65-70.
[6] Wu J, Li G, Peng Y, Et Al. Detection Of Gelatinization Properties Of Millet Using Visible/Near Infrared Reflectance Spectroscopy[J]. Spectroscopy And Spectral Analysis, 2020, 40(10): 3247–3253.
[7] Srivastava S, Mishra H N. Detection Of Insect Damaged Rice Grains Using Visible And Near Infrared Hyperspectral Imaging Technique[J]. Chemometrics And Intelligent Laboratory Systems, 2022, 221: 104489.
[8] M. Elmasry G, Nakauchi S. Image Analysis Operations Applied To Hyperspectral Images For Non-Invasive Sensing Of Food Quality–A Comprehensive Review[J]. Biosystems Engineering, 2016, 142: 53–82.
[9] Mo C, Kim G, Kim M S, Et Al. Discrimination Methods For Biological Contaminants In Fresh-Cut Lettuce Based On Vnir And Nir Hyperspectral Imaging[J]. Infrared Physics & Technology, 2017, 85: 1–12.
[10] Huan K, Chen X, Song X, Et Al. Variable Selection In Near-Infrared Spectra: Application To Quantitative Non-Destructive Determination Of Protein Content In Wheat[J]. Infrared Physics & Technology, 2021, 119: 103937.
[11] Ravikanth L, Jayas D S, White N D G, Et Al. Extraction Of Spectral Information From Hyperspectral Data And Application Of Hyperspectral Imaging For Food And Agricultural Products[J]. Food And Bioprocess Technology, 2017, 10(1): 1–33.
[12] Liu C, Huang W, Yang G, Et Al. Determination Of Starch Content In Single Kernel Using Near-Infrared Hyperspectral Images From Two Sides Of Corn Seeds[J]. Infrared Physics & Technology, 2020, 110: 103462.
[13] Ma J, Cheng J-H, Sun D-W, Et Al. Mapping Changes In Sarcoplasmatic And Myofibrillar Proteins In Boiled Pork Using Hyperspectral Imaging With Spectral Processing Methods[J]. Lwt, 2019, 110: 338–345.
[14] Srivastava S, Mishra H N. Detection Of Insect Damaged Rice Grains Using Visible And Near Infrared Hyperspectral Imaging Technique[J]. Chemometrics And Intelligent Laboratory Systems, 2022, 221: 104489.
[15] Huan K, Chen X, Song X, Et Al. Variable Selection In Near-Infrared Spectra: Application To Quantitative Non-Destructive Determination Of Protein Content In Wheat[J]. Infrared Physics & Technology, 2021, 119: 103937.
[16] Zhang J, Guo Z, Ren Z, Et Al. Rapid Determination Of Protein, Starch And Moisture Content In Wheat Flour By Near-Infrared Hyperspectral Imaging[J]. Journal Of Food Composition And Analysis, 2023, 117: 105134.
[17] Achata E M, Esquerre C, Ojha K S, Et Al. Development Of Nir-Hsi And Chemometrics Process Analytical Technology For Drying Of Beef Jerky[J]. Innovative Food Science & Emerging Technologies, 2021, 69: 102611.
[18] Jin H, Li L, Cheng J. Rapid And Non-Destructive Determination Of Moisture Content Of Peanut Kernels Using Hyperspectral Imaging Technique[J]. Food Analytical Methods, 2015, 8(10): 2524–2532.
[19] Sun J, Wang G, Zhang H, Et Al. Detection Of Fat Content In Peanut Kernels Based On Chemometrics And Hyperspectral Imaging Technology[J]. Infrared Physics & Technology, 2020, 105: 103226.
[20] Araújo M C U, Saldanha T C B, Galvão R K H, Et Al. The Successive Projections Algorithm For Variable Selection In Spectroscopic Multicomponent Analysis[J]. Chemometrics And Intelligent Laboratory Systems, 2001, 57(2): 65–73.
[21] Yu K-Q, Zhao Y-R, Liu Z-Y, Et Al. Application Of Visible And Near-Infrared Hyperspectral Imaging For Detection Of Defective Features In Loquat[J]. Food And Bioprocess Technology, 2014, 7(11): 3077–3087.
[22] Wang Z, Fan S, Wu J, Et Al. Application Of Long-Wave Near Infrared Hyperspectral Imaging For Determination Of Moisture Content Of Single Maize Seed[J]. Spectrochimica Acta Part A: Molecular And Biomolecular Spectroscopy, 2021, 254: 119666.
[23] Wang Z, Chen J, Fan Y, Et Al. Evaluating Photosynthetic Pigment Contents Of Maize Using Uve-Pls Based On Continuous Wavelet Transform[J]. Computers And Electronics In Agriculture, 2020, 169: 105160.